International Journal of Pure and Applied Physics
ISSN 0973-1776 Volume 6, Number 2 (2010), pp. 229–241

http://www.ripublication.com/ijpap.htm

Avalanche Breakdown Characteristics of Wide Band GaP vis-à-vis Low Band Gap Junctions and High RF Power/Low Noise Generation in ZnS DD IMPATTs

[1]Shankar P. Pati, [2]Pravash R. Tripathy and [3]Santosh K. Dash

[1]National Institute of Science and Technology, Palur Hills, Berhampur-761008, Orissa, India
[2]Purushottam Institute of Engineering & Technology, Rourkela, Orissa, India
[3]Government Women's College, Sambalpur, Orissa, India
E mail: prof_sppati@yahoo.co.in

Abstract

Ionization threshold in a semiconductor is determined through the value of band gap energy (E_g, < 1 eV to > 5 eV), which monitors the avalanche breakdown phenomenon of corresponding reverse biased p-n junctions. Further the p-n junction under avalanche breakdown can generate high frequency (hf) power (between 10 and 400GHz and beyond) in Impatt mode, as negative resistance oscillator, performance of which again depends on band gap energy of the semiconductor. Computer aided studies on breakdown and hf performance characteristics of flat DD (p^+pnn^+) Impatts based on conventional materials with moderate band gap energy (Si, GaAs and InP having E_g=1.12, 1.36 and 1.26 eV respectively) as well as wide band gap semiconductors (ZnS, SiC and GaN, with respectively values of E_g =3.68, 2.9 and 3.4 eV) are presented. The p-n junctions of materials having wide band gap energy needs sufficiently high reverse electric field/reverse bias voltage to initiate avalanche breakdown, as compared to the same for materials with low gap. For 3 micron p^+p-nn^+ type flat doped junction, the breakdown field and breakdown voltage for ZnS diode become 170 V/micron and 661 V respectively as against 40 V/micron and 72 V for corresponding Si junction. Similar trend has been observed for SiC, GaN and InP, GaAs diode junctions. The rf analysis of the corresponding Impatt diodes shows that the Device efficiency (21.1%) and negative resistance (0.228×10^{-10} Ω.m^2) for 60 GHz (1 micron) ZnS DDRs are respectively around 1.9, 2.4 times of the values of the same parameters of corresponding Silicon DDR. The inherent avalanche noise associated with ZnS diode has been computed to be only 7% of the noise generated in Si Impatt diode. The performance of ZnS diode is also compared

with diodes based on GaAs, InP, GaN and SiC diodes. The computed value of efficiency & rf power output remains low, noise level becomes high for GaAs, InP, SiC and GaN devices compared to ZnS DDD. Computed values of rf power from 60 GHz Si, GaAs, InP, SiC, GaN and ZnS DDRs have been found respectively to be 18.9, 66.65, 119.95, 1532.7, 979.99 and 1987.4 W**.** RF power generation also have been investigated by considering respective diode area to be 50a, 10a, 5a,2a, and a where a is $10^{-8}m^{-2}$ for different frequency ranges (11 GHz-140GHz) for ZnS-based IMPATTs which indicates similar trend of high rf power realization from ZnS DDDs in this entire frequency range.

Indexing Terms: Band Gap Energy, ZnS, GaN, SiC, InP, GaAs, Si, Flat DDD, Impatt, mm-power, Avalanche Noise.

Introduction

Ionization threshold in a semiconductor is determined through the value of band gap energy (normally the value of band gap energy, E_g, remains in the range of 0.66 eV to 5.1 eV for practical semiconductors), which monitors the avalanche breakdown phenomenon of reverse biased p-n junctions based on the same semiconductor. Further reverse biased p-n junction under avalanche breakdown can generate high frequency (hf) power (fundamental frequency ranges between 10 and 400 GHz) in impatt mode, as negative resistance oscillator, performance of which is supposed to depend on band gap energy of the semiconductor. Under harmonic mode the frequency can be still pushed to 1000 GHz, which is usually not achievable by any other solid state semiconductor device. Further advantage of impatt class of device is that the junction device can be fabricated from any semiconductor as the device physics is not typical to particular semiconductor. The negative resistance is produced due to combined phenomena of transit time delay and avalanche phase delay, making the total phase delay between rf current and voltage between $\pi/2$ and $3\pi/2$. The efficiency and rf power output fall when the frequency is pushed to mm-wave/sub-mm-wave bands. Research work is being carried out by different groups of scientists/engineers to enhance the efficiency and mm-wave power from this class of device even at beyond mm-wave frequencies. New materials are being studied and explored for impatt diodes with a view to achieve the above mentioned objectives. The indication from report of better microwave performance from GaAs and InP impatt over silicon diode due their higher band gap provides motive to study the device characteristics of wide gap semiconductor based impatt diodes vis-à-vis impatt diodes fabricated from narrow gap semiconductor. The authors have selected ZnS, SiC & GaN (respective values of E_g =3.68, 2.9 and 3.4eV) as prospective wide band semiconductors and considered Si, InP & GaAs (having E_g=1.12, 1.36 and 1.26 eV respectively) as moderate band gap semiconductors and compared breakdown as well as hf characteristics of p-n junction impatts with above mentioned base semiconductors. The properties of ZnS impatt diodes are observed to excel over the rest. This has given reasons to the authors to provide due emphasis to ZnS as one

prospective material for high efficiency and high rf power generation associated with low noise. Since the device technology is now very advanced and a lot of experimental reports are available on Silicon Impatts, first the properties of ZnS Impatts are compared with those of Silicon diodes.

A review of recent reports [1-4] on high field transport properties and ionization rate data in ZnS indicate some interesting features like very high value of electron ionization rate at electric field above 1.5×10^8 V/m and its sharp fall below this field. These properties are supposed to identify ZnS as a prospective material for impatt device. Flat doped ZnS impatt diodes ($p^+p\text{-}nn^+$) have been analyzed for a wide range of doping/frequencies through use of a three phase generalized computer algorithm, which can be used to compute microwave/mm-wave properties and also to estimate the generation of avalanche noise for any form of impatt represented in figure 1. The results have been compared with Si Impatts designed for corresponding frequencies. The results indicate high values of breakdown electric field (E_m) and breakdown voltage (V_B) for ZnS diode. The avalanche zone becomes localized leading to possible realization of optimum high efficiency (η > 28% at 18 GHz) and enhanced value of diode negative resistance (Z_r). High V_B would make the diode capable of handling high power and high η and Z_r help in producing high rf power. In addition the computed value of mean square avalanche noise voltage (N_V) and Noise measure (NM) are observed to be lower by an order of magnitude compared to corresponding conventional devices based on common semiconductors. However, the advantages of ZnS impatts are observed to be moderated at frequencies beyond 140 GHz. Thus ZnS may prove to be a promising high E_g material for use in Impatt diode fabrication in order to realize high rf power with high η and low noise form X-band to D-band (10-140 GHz).

Analysis also has been carried out for Impatt diodes based on GaAs & InP low band gap materials and SiC & GaN wide band gap materials IMPATTs. A comparative account of the rf performance of the devices are presented in this paper which indicates possibility of high mm-wave power generation associated with low noise from ZnS devices compared to Si, GaAs, InP, SiC and GaN-based Impatts.

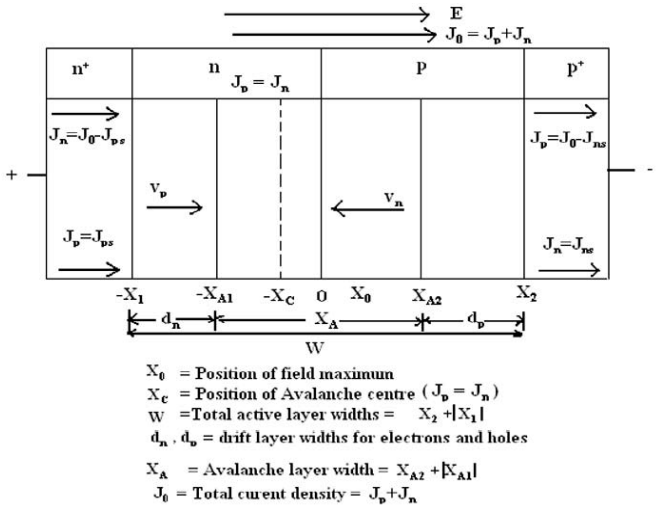

Figure 1: Schematic Double Drift Structure of Impatt Diode.

Theory and Simulation Method

Extracting the values of electron ionization rate (α) at different electric field values [2], a usual exponential ($\alpha=a.\exp(-b/E^{\gamma})$ as well as high order polynomial form ($\alpha=a_0+a_1E+a_2E^2+a_3E^3+\ldots.+a_nE^n$) of equations for α~E, are framed following usual curve fitting technique. The values of 'a', 'b' and γ in the exponential form and those of a_1 to a_8 are determined/used for the high field and low field zones. The drift velocities are taken from [4]. The electron and hole ionization rate are taken to be equal as ZnS is a very wide band gap semiconductor. Ionization rate, drift velocities and other material parameters for other semiconductors are taken from recent available experimental reports.

A double iterative computer method to solve Poison, Carrier Continuity and space charge equations simultaneously subject to fulfillment of boundary conditions in electric field and carrier currents has been framed ensuring speedy convergence.

The basic equations for DC analysis are,

Poisson's equation, $$\frac{\partial E}{\partial x} = \frac{q}{\in}(N_D-N_A+p-n) \quad (1)$$

and the current continuity equation is given by,

$$\frac{1}{q}\frac{\partial J_p}{\partial x} = g = -\frac{1}{q}\frac{\partial J_n}{\partial x} \quad (2)$$

Where $$g = \alpha_n n \nu_n + \alpha_p p \nu_p \quad (3)$$

Taking the drift velocity ~ field variation to be represented by,

$\nu_{n,p} = \nu_{sn,sp}[1-\exp(-\mu_{n,p}E/\nu_{sn,sp})]$

Combined space charge equation can be written as,

$$q\frac{\partial(p-n)}{\partial x} = -q(\alpha_n-\alpha_p)(p-n)+J\left(\frac{\alpha_n}{\nu_p}+\frac{\alpha_p}{\nu_n}\right)+\left\{\frac{J_p\mu_p}{\nu_p}\left(\frac{1}{\nu_{sp}}-\frac{1}{\nu_p}\right)-\frac{J_n\mu_n}{\nu_n}\left(\frac{1}{\nu_{sn}}-\frac{1}{\nu_n}\right)\right\}\frac{\partial E}{\partial x}$$

$$= -q(\alpha_n-\alpha_p)(p-n)+J\left(\frac{\alpha_n}{\nu_p}+\frac{\alpha_p}{\nu_n}\right)+\frac{\partial E}{\partial x}.K \quad (4)$$

Where $K = \frac{J_p\mu_p}{\nu_p}\left(\frac{1}{\nu_{sp}}-\frac{1}{\nu_p}\right)-\frac{J_n\mu_n}{\nu_n}\left(\frac{1}{\nu_{sn}}-\frac{1}{\nu_n}\right)$ is regarded as correction factor and can be evaluated from velocity – field characteristics in any semiconductor.

The equations (1), (2) and (4), which consider only drift current, are modified to incorporate drift and tunnel currents. [5, 6]

The diode structural parameters are optimized first to obtain optimum punch through factor and bias current density through dc analysis. The dc analysis gives E_m, V_B, drift voltage drop (V_D), normalized avalanche zone (x_A/W), breakdown electric field and voltage (E_m & V_B), normalized avalanche zone (x_A/W), qualitative value of

device efficiency (η) etc. [8]. The edges of the depletion zone are also determined accurately from this analysis.

The next phase of the computation has been designed for computation of RF properties of the optimized diodes over a wide band of frequencies. Implicit second order device equations on diode resistance and susceptance are framed based on Runge-Kutta approach. [5, 6]

The data obtained from the DC analysis are used as input for the high frequency analysis of the diode. The high frequency device equation on device impedance can be splitted to equations on diode resistance, $R_0(x)$, and diode susceptance, $X_0(x)$, as,

$$\frac{\partial^2 R_0}{\partial x^2} + (\alpha_n - \alpha_p)\frac{\partial R_0}{\partial x} - \frac{2r\omega}{\bar{v}}\frac{\partial X_0}{\partial x} + \left[\frac{\omega^2}{\bar{v}^2} - H(x)\right]R_0 - \frac{2\bar{\alpha}\omega}{\bar{v}}X_0 = \frac{2\bar{\alpha}}{\bar{v}\varepsilon} \qquad (5)$$

$$\frac{\partial^2 X_0}{\partial x^2} + (\alpha_n - \alpha_p)\frac{\partial X_0}{\partial x} + \frac{2r\omega}{\bar{v}}\frac{\partial R_0}{\partial x} + \left[\frac{\omega^2}{\bar{v}^2} - H(x)\right]X_0 + \frac{2\bar{\alpha}\omega}{\bar{v}}R_0 = -\frac{\omega}{\bar{v}^2\varepsilon} \qquad (6)$$

$$\text{With H(x)} = \frac{2j}{\bar{v}\varepsilon}\frac{\partial\bar{\alpha}}{\partial E} + \frac{qr_+}{\bar{v}\varepsilon}\frac{\partial}{\partial E}\left[g_{Tn}(x) + g_{Tp}(x')\right] + \frac{\partial}{\partial E}(\alpha_p - \alpha_n)\frac{\partial E_m}{\partial x}$$

The equations (5) and (6) are solved simultaneously by using modified Runge-Kutta method subject to fulfillment of boundary conditions at both the edges of the depletion layer [8]. The expected rf power delivery from the diode can be computed using the relation, $P_{RF} = (V_{RF})^2 |G_p| \times A/2$. The Power Density, P_A, is taken as P_{RF}/A, where 'A' is area of cross section of the device.

A very fast automatically converging double iterative computer method initiated from left edge of the depletion layer has been framed for such analysis. Iteration over the chosen values of diode resistance and susceptance at left edge are carried out till usual boundary conditions are satisfied at the right edge of the diode. The final solutions at various frequencies for different diodes have been studied to assess the rf properties. The high frequency analysis gives the band width (BW), peak frequency (f_p), negative device conductance (G_p), negative resistance (Z_{rp}), negative resistance profile, avalanche phase delay (θ_A), transit time delay (θ_T)and other related parameters [9]. Further the negative series resistance generation profile, R(x), i.e. variation of ẽ/ĩ across the depletion zone, can be obtained for the analysis, which indicates some interesting features. For a DDR, this negative resistance profile shows a double peak nature. The avalanche phase delay can be computed from the position of peak in the negative resistance profile and is used further fine tuning in optimization process through minor changes in the structural parameters of the diode leading to values of θ_A as θ_T around 0.5π each. A value of θ_A below 0.4π and above 0.6π indicates poor design for the diode.

The third phase of analysis has been framed to assess the avalanche noise. The noise generation rate at any particular space point (x′) is given by,

$$\gamma_N(x') = n(x')\alpha_n(x')v_n(x') + p(x')\alpha_p(x')v_p(x') \qquad (7)$$

Taking the noise generation at any particular space step, the second order device noise equations on noise field can be framed which when splitted into real and imaginary noise fields, gives the equations as follows.

$$\frac{\partial^2 e_R}{\partial x^2}+(\alpha_n-\alpha_p)\frac{\partial e_R}{\partial x}-\frac{2r\omega}{\bar{v}}\frac{\partial e_X}{\partial x}+\left(\frac{\omega^2}{\bar{v}^2}-H\right)e_R-\frac{2\bar{\alpha}\omega}{\bar{v}}e_X=\frac{2r_+q\gamma_N}{\bar{v}\varepsilon} \tag{8}$$

and

$$\frac{\partial^2 e_X}{\partial x^2}+(\alpha_n-\alpha_p)\frac{\partial e_X}{\partial x}+\frac{2r\omega}{\bar{v}}\frac{\partial e_R}{\partial x}+\left(\frac{\omega^2}{\bar{v}^2}-H\right)e_X+\frac{2\bar{\alpha}\omega}{\bar{v}}e_R=0 \tag{9}$$

These equations are solved simultaneously with the help of another double iterative computer method subject to boundary conditions [7]. The noise field is integrated over x and then over x′ to determine total noise impedance $Z_T(x', \omega)$ from which mean square noise voltage can be computed.

$$\Rightarrow \frac{\langle V^2\rangle}{df}=2q^2A\gamma_N\int|Z_T(x',\omega)|^2\,dx' \tag{10}$$

From the knowledge of mean square noise voltage, noise measure (NM) of the diode can be computed from the expression.

$$\text{NM} = \frac{\langle V^2\rangle|df}{4KT(-Z_R)} \tag{11}$$

Where K is the Boltzmann constant, T is the junction temperature (taken to be 473^0K) and $-Z_R$ is the total negative diode resistance.

The avalanche noise generation is analyzed with the analogy of heating a bar at various points giving a vibration profile just like the noise generation element at any point along the depletion zone generate a noise field profile. Integrating each profile over the depletion zone one gets the final noise for the diode. The final solution gives the mean square noise voltage at various frequencies, the noise measure and the noise generation profile. The results of dc, rf, and noise analysis are studied for different diodes structures under various operating conditions have been studied are presented in this paper.

Flat profile Double Drift Impatt Diode for Si and ZnS are designed and optimized for 12, 35, 60, 94 and 140 GHz, which are recognized as atmospheric widow frequencies. The diodes with GaAs, InP, SiC and GaN are designed and optimized for operation in 60 GHz. The diode structural parameters in each case are modulated to achieve minimum extension of avalanche zone, optimum punch through factor, highest η and maximum value of negative resistance. Closest location of electric field maximum to junction plane and near central location of peak of r(x) profile in the drift region [8, 11] are the indicative parameters for good optimization.

Results and Discussion

The results are presented in the following three sections.

(i) Performance of ZnS and Si Impatts

First the method outlined above has been used for the analysis of experimentally realized diodes appeared in literature. The results obtained from our analysis of these experimentally reported diodes are observed to be tallying to very good extent with actual experimental results, which appeared in journals. Then the authors present a comparative account of ZnS and Si p-n junctions, their breakdown characteristics and rf properties in IMPATT mode of operation. The diode parameters and the results of the analysis for ZnS diodes are presented in Tables 1 and 2 and those for Si diodes are shown in Table 3. The frequency vs negative conductance and frequency vs. noise voltage are shown in figures 2 and 3 respectively. The diodes have been designed/optimized for doping concentrations in the range of 2×10^{22} to $6.5\times10^{23}/m^3$ corresponding to frequency range of 8 to 150 GHz. The diodes for atmospheric window frequencies are numbered as D1 to D5. For D1 (12 GHz) the V_B (avalanche breakdown voltage) becomes 661 V as against 105 V for corresponding Si DDD. The magnitude of breakdown electric field maximum for ZnS D5 (140 GHz) is observed to be 2.224×10^8 V/m as against corresponding value for Silicon diode (for 140 GHz), $E_m=7.12\times10^7$ V/m (Table 3). The electron ionization rate, α, [1-4] at the breakdown field around 2×10^8 V/m for ZnS is few times more than the value of α for Si diode at the breakdown field. Further α, for ZnS, falls very rapidly below electric field of 1.5×10^8 V/m and becomes near zero at 10^8 V/m. However for Si, α~|E| varies in moderate exponential form. These facts localizes the avalanche zone to very thin width, only 8% of the total depletion zone (for ZnS, D1) as compared to 45% for corresponding Si for 12 GHz operation, which, in turn enhances the value of efficiency for ZnS DD to 28.3% for D1 (this value is close to theoretical optimum value of 30%) and 22.0% at 94 GHz (D4) as against respective values of 13 and 9.43 % for Si devices. It can be mentioned here (our analysis) that even the multilayered lo-hi-lo high efficiency Si DD can give efficiency of 15.2% at 94 GHz. Thus the drift zone which contributes to generation of useful hf power becomes wide in case of ZnS diodes.

The results of rf analysis also exhibit some interesting results. The frequency (f_p) at which the value of –G becomes the highest ($G_{p)}$ is mentioned against each diode (Table 2). The value of G_p is found to higher for ZnS DD by 1.5-2.0 times than corresponding Si devices. The values of negative resistance (Z_{rp}) are two to three times higher for ZnS diode compared to those in Si device for D1, D2, D3, D4 and D5. The wide drift zone becomes responsible for higher values of $-Z_r$ and G_p for ZnS DD. It can be seen from figure 2 (Frequency vs –G plot) for D5 that the BW is seen to be very high for ZnS Impatts which make it possible for the diodes to generate rf power over wide range of frequency. The analysis can be used to compute the negative resistance profile, R(x) profile, within the diode active zone. This profile can indicate the contribution of each space step towards microwave generation. Investigation of R(x) profiles (not shown) showed usual double peak nature for both ZnS and Si with one peak located each in ‘n’ and ‘p’ low doped region. Fine structure optimization process can be accommodated at this stage such that the peak of the R(x)

profile is located near to the centre of the drift region. It is observed that the magnitudes of the peak for ZnS DDs are more than twice than those for Si. Further, the extension of active zone, within which negative resistance is generated, spreads to entire drift zone for ZnS DD. This explains the reasons for higher magnitude of Z_r in case of ZnS DD compared to Si DD for all the frequencies considered here.

The frequency vs. mean square noise voltage ($N_v=<v^2/df>$), plots shown in fig 3 for ZnS and Si devices, shows usual nature with peak value of N_v occurring at the transition frequency (at which the diode conductance becomes negative). The values of N_v at f_p for ZnS and Si for all the design frequencies can be compared from Tables and graph and it can be observed that the value of N_v is lower by more than an order of magnitude for ZnS DD in each case as compared to corresponding Si DD (as for example the magnitude of N_v for 12 and 94 GHz ZnS impatt diodes, is only 3% and 5% respectively of 12 GHz and 94 GHz Si. The noise measure ($<v^2/df>/4kT|Zr|$) in dB for ZnS diode is only 1.4 at 60 GHz as against 26.3 dB for corresponding Si DD. Possible rf power output also has been calculated for each diode with ZnS and Si and are mentioned in Tables 2 and 3. The corresponding diode area, considered for power calculation, is shown in Table 2. The power output from ZnS diode is seen to be 100-150 times corresponding Si Devices. The power calculation seems to be realistic as the computed value of 94 GHz Si DDR is found to be 8.98 W, since actual power obtained from Si SDR diode at 94 GHz has been reported to be more than 1 W. The power from DDR is supposed to be 4-6 times than the corresponding SDR diode as the breakdown voltage, drift region, diode resistance, efficiency are much higher in DD than SD diode.

However when the design frequency is pushed beyond 150 GHz, the advantages of ZnS device get moderated and the performance becomes similar to Si Diode. At 220 GHz, the values of x_A/W and $-G_p$ become nearly equal for both ZnS and Si. Further, it can be seen from the Tables that the ZnS diode needs higher doping and lower depletion zone compared to Si for the same design frequency as drift velocity is lower for ZnS than that for Si [8]. The depletion zone for 220 GHz ZnS would be lower to 100 nm as against 240 nm for Si and the corresponding doping will be $1.2\times10^{24}/m^3$ for ZnS and $6.0\times10^{23}/m^3$ for Si. These facts may lead to greater difficulties in fabrication of ZnS impatts beyond 150 GHz. The results are however very encouraging in support of use of ZnS semiconductor for impatt diode fabrication at least up to 150 GHz.

(ii) Performance of ZnS diodes vis-à-vis GaAs and InP diodes:

GaAs and InP are two conventional semiconductors having low to moderate band gap and practical reports on impatt fabrication from them have appeared in literature. The band gap energy of GaAs and InP are higher to that for Si but remains much lower to that for ZnS. The authors have thus plan to present some results of analysis for GaAs, InP and ZnS DDDs. The frequency of design for this study has been taken as 60 GHz. The diode structural parameters and some dc properties of Si, GaAs, InP and ZnS 60 GHz DDDs are presented in Table 4. In Table 5 the high frequency properties for these cases are shown. It may be seen that the performance of GaAs and InP DDDs are better than those for Silicon DDD. Higher E_g in GaAs and InP makes the breakdown field higher and causes high values of ionization rate in the avalanche

zone resulting in thinner avalanche zone. ZnS, having very high value of E_g (3.68eV), the breakdown field becomes several times more than Si, GaAs and InP diodes, which in turn enhances the ionization rate by orders of magnitude. Thus the avalanche zone is localized to only 15.1% of diode width as against more than 43% for Si, GaAs and InP diodes. The efficiency has been computed to become 24.1 % for ZnS diode (60 GHz). Even the multilayered lo-hi-lo Si DD has been reported to provide efficiency 19% at 60 GHz. The breakdown voltage for ZnS DD is also very high compared to Si, GaAs and InP diodes (Table 4). Since input power is related to breakdown voltage, the efficiency for ZnS is higher and diode negative conductance (Figure 4) becomes the highest for ZnS DDD, the rf power from ZnS diode may become higher by several times compared to GaAs and InP diodes.

Avalanche noise is also assessed for different diodes. The mean square noise voltage ($\langle V^2/df \rangle$) and noise measure have been computed and shown in Figure 5. It is quite encouraging to note that in case of ZnS diode, the mean square noise voltage becomes less by an order of magnitude compared to Si, GaAs and InP diodes. For X-band diode the breakdown voltage and efficiency respectively becomes 661 V and 28.8% (nearly equal to theoretical optimum value in case of Impatt diode for 50% rf modulation). The mean square noise voltage in X band ZnS DD is lower by nearly two orders of magnitude compared to other diodes. However on moving towards right in frequency scale the superiority of ZnS is observed to be minimized beyond 140 GHz. The computed value of rf power output in ZnS 60 GHz Impatt diode is observed to be higher by nearly two orders of magnitude (Table 5).

(iii) Avalanche Breakdown Characteristics of ZnS, SiC and GaN Diodes:

Prospects of other high band gap materials (SiC and GaN) have been reported [9, 10]. The SiC and GaN p^+pnn^+ diodes designed for 60 GHz operation are analyzed by us and the avalanche breakdown characteristics are given in Table 6 along with those of ZnS diode. Though the breakdown voltage is high in case of SiC and GaN, the ionization rate at electric field of 2×10^8 V/m is seen to be nearly half than that for ZnS. This fact makes the avalanche zone very wide (60 % for GaN as against 15% for ZnS). Thus the value of diode negative resistance has been observed to be low and avalanche noise to be high in GaN and SiC diodes compared to ZnS. Thus amongst the three wide band gap semiconductors, which are considered here, the ZnS Impatt diodes are expected to provide higher power and lower avalanche noise as compared to SiC and GaN Impatts. It can be seen from Table 6 that amongst the three wide band semiconductors considered here, the ZnS device nearly 1.5 to 2.0 times RF power than the same for SiC and GaN Impatts (60 GHz operation)

Table 1: Breakdown Characteristics of ZnS n^+npp^+ DDRs.

Doping (m^{-3})	Width micron	J_0 (A/m^2)	E_m (V/m)	V_B (V)	V_D (V)	X_A/W (%)	η (%)
2×10^{22} (D1)	2.60	10^7	1.6895×10^8	660	593	8.12	28.3
9×10^{22} (D2)	1.35	1.5×10^8	1.8820×10^8	301	296	12.1	26.0
1.5×10^{23}(D3)	0.83	2.0×10^8	1.9722×10^8	182	139	16.1	23.5

4.5×10^{23}(D4)	0.55	2.0×10^{8}	2.21×10^{8}	151	114	18.5	22.0
6.5×10^{23}(D5)	0.22	5.0×10^{8}	2.264×10^{8}	127	92	21.8	20.4

Table 2: RF Characteristics of optimized ZnS DDRs in IMPATT Mode.

Diode No.	Diode Area $\times10^{-8}m^{-2}$	Peak Frequency GHz (f_p)	Peak $-G_p$ $\times10^{6}$ S/m^2	$-Zr$ at f_p $\times10^{-7}$ $\Omega.m^2$	$+Rs$ $\times10^{-7}$ $\Omega.m^2$	$<V^2>/df$ at f_p, $\times10^{-18}V^2.s$	RF Power (P_{RF}) W
D1	50	11	0.347	0.701	0.179	18.7	9447.0
D2	10	35	6.0	0.512	0.128	4.136	6795.0
D3	5	60	9.6	0.221	0.0223	0.547	1987.4
D4	2	94	13.8	0.102	0.012	0.0378	786.6
D5	1	140	15.3	0.068	0.0087	0.0113	308.4

Table 3: Some Properties of Silicon DDRs at corresponding frequencies of D1 to D5.

Diode No.	E_m, $\times10^7$ V/m	V_B, V	η, %	Peak, $-G_p\times10^6$ S/m^2	$<V^2>/df$ at f_p $\times10^{-18}V^2.s$	P_{RF} (W)
D1, 11 GHz	3.65	105	13.0	0.26	700.6	174.0
D2, 35 GHz	4.77	41.1	12.1	3.20	39.9	67.5
D3, 60 GHz	5.72	24.5	10.6	7.97	7.0	18.9
D4, 94 GHZ	6.53	18.5	9.43	10.5	3.5	8.98
D5,140 GHz	7.12	12.6	7.6	13.5	0.879	2.67

Table 4: Diode Structural Parameters/DC Properties of Si, GaAs, InP and ZnS p^+pnn^+ DDRs Designed for Operation at 60 GHz.

Material	E_g eV	Doping (m^{-3})	Width μm	E_m (V/m)	V_B (V)	X_A/W (%)	η (%)
Si	1.12	7.3×10^{22}	0.94	5.72×10^{7}	24.5	48.7	10.6
GaAs	1.36	5.2×10^{22}	1.20	4.55×10^{7}	36.0	39.9	13.3
InP	1.26	8.2×10^{22}	1.07	6.38×10^{7}	46.9	37.8	13.8
ZnS	3.68	1.5×10^{23}	0.82	1.94×10^{8}	185	15.3	24.1

Table 5: Microwave Properties of Si, GaAs, InP and ZnS IMPATTS at 60 GHz.

Material	Peak Frequency, GHz (f_p)	Peak $-G_p$ $\times10^6$ S/m^2	$-Zr$ at f_p $\times10^{-7}$ $\Omega.m^2$	$<V^2>/df$ at f_p, $\times10^{-18}V^2.s$	Noise Measure at f_p (dB)	P_{RF} (W)
Si	60	8.97	0.0626	7.0	26.3	18.9
GaAs	59	8.23	0.115	13.7	25.2	66.6
InP	60	8.67	0.124	10.4	23.9	119.5
ZnS	59	9.6	0.221	0.547	1.40	1987.4

Table 6: Breakdown Characteristics of some Wide Band Gap Junctions.

Material	E_g	$\alpha(m^{-1})$ at E= 2×10^8 V/m	Doping /m^3	E_m (V/m)	V_B (V)	X_A/W (%)	η (%)	P_{RF} (W)
SiC	2.9	2.0×10^6	1.5×10^{23}	2.01×10^8	202	47.5	12.1	1532.7
GaN	3.4	2.2×10^6	1.5×10^{23}	2.05×10^8	169	62.2	7.3	979.99
ZnS	3.68	4.3×10^6	1.5×10^{23}	1.98×10^8	185	15.3	24.1	1987.4

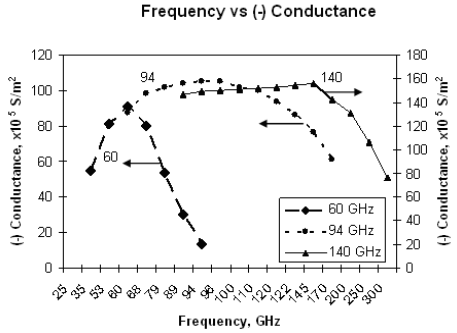

Figure 2: Frequency vs (-) Conductance plots for ZnS Impatts at 60, 94 and 140 GHz.

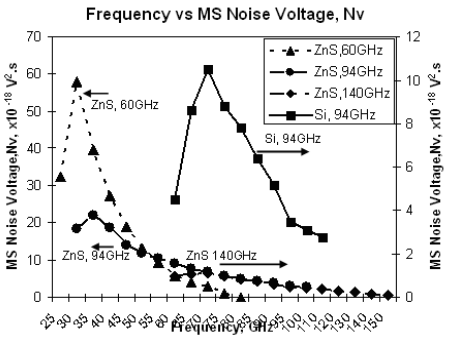

Figure 3: Frequency vs Mean Square Noise Voltage, Nv, of ZnS (at 60, 94 and 140 GHz) and of Si (94 GHz) DD Impatts.

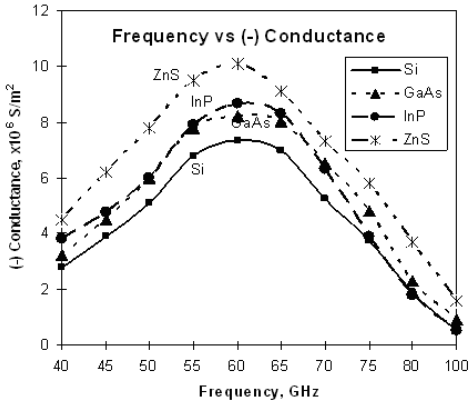

Figure 4: Frequency vs Negative Conductance for 60 GHz Si, GaAs, InP and ZnS flat Double Drift Diodes.

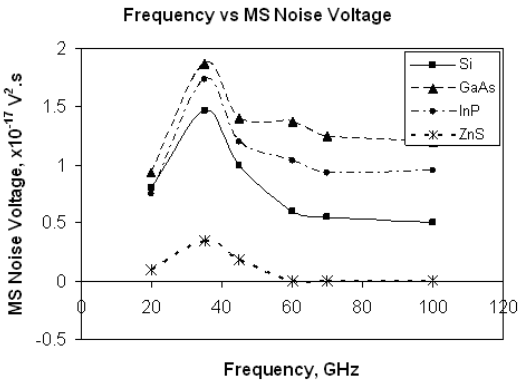

Figure 5: Mean Square Noise Voltage vs Frequency for above mentioned flat doping profile double drift diodes.

Conclusion

Conclusion may be derived from the results mentioned above that ZnS can become a new and very prospective material for impatt diode fabrication, which can produce high mm-wave power with sufficiently high efficiency and with very low avalanche noise. ZnS may become a prospective material for generation of high mm wave power, high efficiency and low noise in impatt mode because of high value of V_B (increasing the input power handling capacity), thin avalanche zone and high drift voltage drop (increasing device efficiency), high values of –G and $-Z_r$ (increasing output rf power) and low values of N_v and NM (decreasing avalanche noise generation). The performance of ZnS diode is also compared with diodes based on GaAs, InP, GaN and SiC diodes. The computed value of efficiency & rf power output remains low, noise level becomes high for GaAs, InP, SiC and GaN devices compared to ZnS DDD.

Acknowledgement

Prof. S. P. Pati wishes to express sincere thanks to AICTE for grant of 'Emeritus Professor' in his favour to support this work.

References

[1] Reigrotzki, M., Redmer, R., Lee, I., Pennathur, S. S., Dur, M., Wager, J. F., Goodnick, S. M., Vogi, P., Eckstein, H. and Schattke, W., 1996, "Impact ionization rate and high-field transport in ZnS with nonlocal band structure," J. Appl. Phys., Vol. 80(9), pp 5054-60.

[2] Reigrotzki, M., Madureina, J. R., Kuligk, A., Fitzer, N., Redmer., R., Goodnick, S. M., Dur, M., Schattke, W., 2002, "Impact ionization and high-field effects in wide-band-gap semiconductors," Physica B 314, pp 52-54.

[3] Cao, J. C., 2004, "Nonparabolic multivalley balance-equation approach to high-field electron transport and impact ionization in ZnS: Comparison with full-band Monte Carlo simulation," Physical Review, B 69, pp 165203-1 to 6.

[4] Fitzer, N., Kuligk, A., Redmer, R., Stadele, M., Goodnick S. M., and Schattke W.,2003, "Full band Monte Carlo simulation of high-field electron transport in GaAs and Zns, Physical Review," Vol. B 67, 201201-1 to 4.

[5] Dash G. N., and Pati, S. P., 1992, "A generalized simulation method for MITATT mode operation and studies on the influence of tunnel current on Impatt properties," Semicond. Sc. And Technol, Vol. 7, pp 222-230.

[6] Pati, S. P., Banerjee, J. P., and Roy, S. K., 1991, "High frequency numerical analysis of Double Avalanche Region IMPATT diode," Semicond. Sc. And Technol, Vol. 6, pp 777-783.

[7] Dash, S. K., and Pati, S. P., 2002, "Effect of optical radiation on mm-wave characteristics and avalanche noise generation in double drift Impatt diodes on opto-sensitive semiconductors," Microwave and Optical Technology Letters, Vol. 33 (4), pp 295-300.

[8] Pati, S. P., and Tripathy, P. R., 2005, "Design consideration of sub mm-wave Silicon DDRs including drift, diffusion and tunnel currents," Proc. Int Workshop on Physics of Semiconductor Devices (IWPSD-2005).

[9] Pattanaik, S. R., Dash, G. N. and Mishra, J. K., 2005, "Prospects of 6H-SiC for operation as an Impatt diode at 140 GHz," Semicond. Sc. And Technol, Vol. 20, pp. 1-6.

[10] Panda, A. K., Pavlidis, D., and Alekseer, E. A., 2001, "Noise Characteristics of GaN based Impatts," IEEE Trans. on Electron Devices, Vol. 48(7).

[11] Pati, S. P., Tripathy, P. R., Dash,S. K., Choudhury, S. K., Purohit, P., Panda A. K.,and Majhi, J.,2010, "Mathematical Analysis and Realistic Simulation Modeling for Thin Impatt Devices," Proc. of MATEIT-2010.